Journal of Applied Sciences and Nanotechnology

Journal homepage: jasn.uotechnology.edu.iq

Synthesis of High-Performance Antibacterial Magnesium Oxide Nanostructures through Laser Ablation

[1]Sara F. Abbas*, [2]Adawiya J. Haider, [3]Sharafaldin Al-Musawi, [4]Bakr A. Taha

[1]Department of Laser and Optoelectronics Engineering, College of Engineering, Al-Nahrain University, Iraq
[2]Department of Applied Sciences, University of Technology – Iraq, Iraq
[3]College of Food Sciences, Al-Qasim Green University, Iraq
[4]Department of Electrical, Electronic and Systems Engineering, Universiti Kebangsaan, Malaysia

A R T I C L E I N F O

Article history:
Received: December, 12, 2023
Accepted: February, 16, 2024
Available online: March, 10, 2024

Keywords:
Laser ablation,
Magnesium oxide,
Nano flake,
Nanotechnology,
Antibacterial activity

Corresponding Author:
Sara Fadhil Abbas
sara.fadhel@nahrainuniv.edu.iq

A B S T R A C T

In this study, we synthesized magnesium oxide (MgO) nano flakes (NFs) through pulsed laser ablation of magnesium ribbons, investigating their potent antibacterial properties for potential biomedical applications. Thorough characterization utilizing advanced analytical techniques verified the phase purity and functionality of the fabricated MgO NFs. Results revealed a distinctive flake-like structure with an average diameter of 100-400 nm and a slender wall thickness of 24 nm. The efficiency of the laser ablation method was validated by EDX imaging, showing high purity in the MgO sample. XRD analysis further confirmed the polycrystalline nature of MgO NFs, with dominant peaks at 2θ values of 38.86°, 59.46°, 62.83°, and 73.87° corresponding to (111), (110), (220), and (311) diffractions, respectively. UV-visible spectroscopy exhibited a broad absorption peak, and Tauc's formula yielded an energy band gap of 5.8 eV. FTIR spectroscopy detected Mg–O–Mg bending vibration, O−H stretching vibration, O=C=O stretching, and O−H bending vibration. Optimized MgO-NFs demonstrated remarkable antibacterial efficacy against both gram-positive Staphylococcus aureus (*S. aureus*) and gram-negative Escherichia coli (*E. coli*) bacteria. Maximum antibacterial activity was observed at a high MgO NFs concentration (200 µg/mL), resulting in 15 mm ±0.5 mm and 16 mm ±0.5 mm inhibition zones for *E. coli* and *S. aureus*, respectively. The minimum inhibitory concentration (MIC) for both pathogens was determined to be 25 µg/mL, emphasizing the promising antimicrobial potential of the MgO NFs.

https://doi.org/10.53293/jasn.xxxxxxxxxxxxxx, Department of Applied Sciences, University of Technology - Iraq.

1. Introduction

Science is currently focused on nanotechnology owing to the wide range of new possibilities in numerous fields of agriculture, food processing, and medicine [1]. The shape and size of colloidal metal nanoparticles play a significant part in several applications [2]. These applications include synthesizing magnetic material, electronic devices, wound healing, antimicrobial, and bio- composites preparation [3]. Nanoparticle (NP) materials are of

fair interest for various applications and studies because of their size-dependent properties. Researchers have given several types of nanoparticles and their derivatives, like nano-metals, high attention because of their potential antibacterial effects [4]. Inorganic nanoparticles, including metals and metal oxides, possess great antibacterial properties and might be alternatives to antibiotics for treating infection [5].

Infection happens after viruses, bacteria, or other microorganisms enter the body and reproduce [6, 7]. One of the most serious issues confronting health systems today is antimicrobial resistance (AMR), which happens when microbes that cause infection are in contact with a medicine that would ordinarily destroy them or prevent their development (i.e., antibiotics) [8]. AMR is caused by bacteria's ability to evolve and adapt to specific treatments [9, 10]. Besides this issue, antibiotics can also have negative consequences on the host, such as allergic responses, immunosuppression, and hypersensitivity [11, 12]. New techniques rely on metal oxide nanoparticles to diversify treatments to prevent the development of resistances as much as possible [13].

Magnesium oxide (MgO) nanoparticles are among the essential minerals for human health [14]. MgO attracted increasing attention in tissue engineering and regenerative medicine applications due to their biocompatibility, biodegradability, and bioactivity [15]. MgO is an insulator/semiconductor typically with a cubic structure [16]. Because of its relatively large band gap of 7.8 eV, MgO has limited applications. MgO NPs have a lower band gap in the range of 5 eV [17]. MgO at the nanoscale has a broad spectrum of bactericidal effects on both bacterial gram strains. It has reduced toxicity and more mammalian bioactivity compared to most metal oxides.

As a result, it might be used as an ingredient in medication composition [18]. Because there are so many uses for MgO nanoparticles and nanocomposite, many publications on their synthesis have been published. Sawai et al. found that MgO exhibited a strong capacity for inhibiting bacteria [19].

The process by which magnesium oxide nanoparticle inhibited bacteria is still not clear. This mechanism may relate to oxygen reacts with the surface of bacteria to produce superoxide radicals gives rise to antibacterial activity. The high reactivity of the additional electrons may harm proteins and phospholipids in the bacterial membrane [19, 20]. MgO NPs are effective in creating reactive oxygen species (ROS) that are important for their antibacterial activity, including hydrogen peroxide (H_2O_2), hydroxyl radicals ($^{\bullet}OH$), and superoxide radicals ($O2^{-}$) hence these radicals also cause rupture of the cell membrane [21-24] the chemical formula represent the production of ROS[25]:

$$e^{-}+O_2 \rightarrow O_2^{*} \quad (1)$$

$$O_2^{*} + O_2^{*} + 2H^{+} \rightarrow H_2O_2+O_2 \quad (2)$$

$$H_2O_2 + e^{-} \rightarrow OH^{-} + OH^{*} \quad (3)$$

MgO NPs also suppress cells by releasing harmful ions (Mg^{2+}) when they enter cells. When these harmful ions come into contact with amino acids (thiol-groups), proteins' regular structures are destroyed, ultimately resulting in cell death [26, 27]. MgO NPs also have an additional inhibitory mechanism that stems from their ability to impede essential enzyme functions in microorganisms. They can impede or slow down the growth of cells by, for example, inhibiting enzymes required for cellular respiration and energy synthesis, which can upset metabolic processes [28]. The whole proposed mechanism illustrated in Fig. 1.

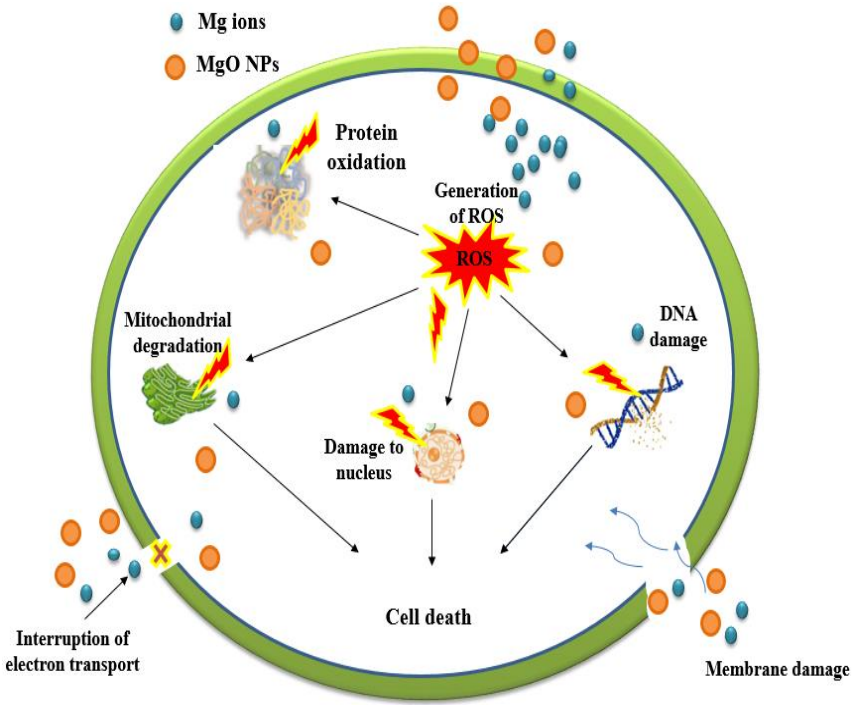

Figure 1: Proposed mechanism of MgO NPs antibacterial action

The antimicrobial mechanism of MgO NPs is a complex process and can be affected by various parameters. Prior findings demonstrated that the antibacterial action of MgO NPs is contingent upon the bacterial strain's specific shape, nature, and size [29, 30]. Marsili et al. described the antibacterial activity of zinc oxide NPs depending on the form of the particles [31]. Though the most prevalent shape of NPs is spherical [10], nano-cubes and nanorods are more effective than other shapes because of their exposed planes and metal oxidation levels [32, 33]. It has been proposed that the ability to kill bacteria of the NPs is correlated with the stability of the planes, with less stable planes and energy required to generate oxygen vacancies [34]. Wang et al. showed that because of their exposed crystal surfaces and capacity for oxidation, nanorods exhibited more bactericidal activity than other forms [35].

Many different preparation paths provide MgO NPs containing sol–gel [36], hydrothermal/solvothermal [37], chemical gas phase deposition [38], aqueous wet chemical method [39], hydrothermal method [40], and so on. Using laser ablation method could overcome many restrictions, such as the requirement of advanced tools, numerous processing stages, additional time, surfactant, template, etc. It delivers essential advantages for biological applications of creating NPs without additional impurities, and the processing setup prices, are not high [33]. The success of the laser-assisted pulsed approach in creating various sizes and forms of nanoparticles, which are employed in many applications, makes it significant in a liquid environment [41, 42]. The method's greatest distinguishing characteristic is the non-equilibrium growth process, brought on by plasma created by laser ablation of a sample in solution. It has exceptionally elevated pressure and temperature [43]. In the present study MgO nano flakes synthesize using a pulsed laser ablation in liquid method. Later, MgO nano flakes characterized their optical, structural, chemical, morphological, compositional, surface charge and particle size. Studying MgO nano flakes effect of antibacterial activity against different tested bacterial' strains gram-positive *S. aureus* and gram-negative *E. coli* bacteria.

2. Experimental Procedure

2.1 Preparation of Magnesium Oxide Nano Flakes

Q-switched Nd: YAG laser (Huafei Tongda Technology-DIAMOND-288 pattern EPLS) was used in our experimentation to ablate of magnesium in liquid. The laser specification was (a wavelength of 1064 nm, frequency equal to 1 Hz, pulse width of 10 ns, and 1000 mJ laser energy). The high-purity magnesium ribbon illustrated in Fig. 2a, (99.95%, BDH chemical Ltd pool, England) was used to produce magnesium oxide NFs by

pulsed laser ablation in water (PLA) method. The magnesium ribbon was cut into strips and lined up together for use in the ablation process as seen in Fig.2b. Magnesium strips were cleaned with methanol and then washed using ultrapure deionized water. After careful cleaning, the Mg strip was used as a target for the PLA experiments and essentially immersed in 5mL of distilled water (DW) in the bottom of a glass container at room temperature. A schematic image summarizes the PLA technique in Fig. 2d. Because of the high laser energy focused on the target, the irradiated area suffered from the fast removal of material confined to the laser spot. The liquid in the container was moved using a magnetic stirrer to avoid shielding effects from the plume due to the plasma in the static liquid and to guarantee homogeneous dispersion of the ejected nanoparticles. The plasma formed by PLA of the target placed in liquid is considered a source of additional force to produce smaller nanoparticles. The interaction of the ablated species with the laser beam may become a source for secondary ablation force, splitting the colloidal species, or even the formation of complex chemical compounds. The DW color turned to milky white resulting from the ablation process to the magnesium target, as seen in Fig. 2c.

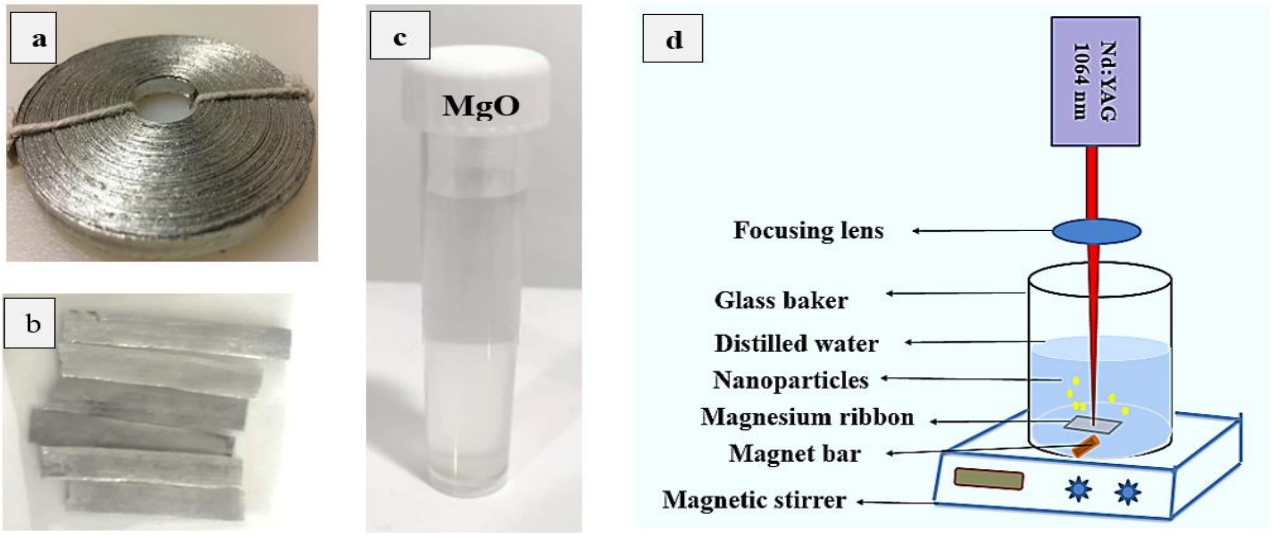

Figure2: (a) magnesium ribbon (b) magnesium ribbon after cutting (c) the white color of the sample after ablation (d) schematic for the manufacture of NFs by PLA of a target in DW.

2.2 Characterization of MgO NFs

MgO NFs were described by X-ray diffraction (XRD) (AERIS PAN alytical, japan). XRD analyses were performed at 40 kV and 30 mA with CuK at 1.5406 Å wavelengths. The samples were examined in two-step increments of 0.05°/s between 20° and 80°. The bond vibrations of NFs were measured using Shimadzu 8000 Series Fourier transform infrared (FTIR) spectroscopy in the 400-4000 cm1 range. The optical absorbance of colloidal nanoparticles (200-800) was estimated using a UV VIS spectrophotometer with a twin beam (Shimadzu UV-1800). The Axia ChemiSEM scanning electron microscope was used to analyze the morphology of the nanostructures. The chemical composition of the material is investigated using X-ray energy dispersions (Axia Chemi). To validate zeta potential and particle diameter, dynamic light scattering (DLS) (Malvern Zetasizer ZS, Malvern, UK) is utilized.

2.3 Antibacterial Activity

Antibacterial activity of the MgO NFs was carried out by agar well diffusion method against two pathogenic bacterial strains namely *S. aureus* (gram-positive) and *E. coli* (gram-negative). Mueller Hinton Agar was used as a nutrient broth. The bacteria had been previously isolated and characterized from Shariati Hospital-Tehran-Iran. The desired bacteria (*S. aureus* or *E. coli*) were dispersed on the Petri dish's surface. Wells at 6 mm diameter were punched out of each agar plate using a sterilized well cutter. After using an electrical spinner to combine the MgO NFs, Different concentrations of the tested MgO NFs (25, 50, 100, 150, and 200) µg/mL were supplementary in a separate hole in the well. Finally, after incubation at 37 °C for 24 h, the inhibition zones were observed around each well and measured (to the nearest mm) to determine the antibacterial activity of MgO NFs.

2.4 Statistical Analysis

The acquired data were statically analyzed using an unpaired t-test with GraphPad Prism 6. The values were presented as the mean ± SD (*p < 0.05; **p < 0.01; ***p < 0.001); n = 3).

3. Results and Discussions

The crystal phases and crystallinity of prepared MgO NFs were investigated by XRD analysis. Two samples of the prepared MgO NFs (10 mL) were dropped on a glass slide by vaporizing the NFs suspension (thickness equal 400 nm approximatly). We took this step to obtain a suitable thickness for X-ray diffraction examination. A typical XRD pattern for the manufactured MgO NFs presented in Fig. 3. Miller indices indicated recorded on top of each diffraction peak. The peaks obtained at 38.86°, 59.46°, 62.83°, and 73.87° attributed to the diffraction from (111), (110), (220), and (311), respectively. These peaks are attributed to the formation of MgO NFs. This demonstrates that the polycrystalline cubic structure of MgO NFs formed. The broadening peaks appeared in the XRD figure. This is related to the XRD peaks that broaden as the crystallite size reduces from bulk to nanoscale dimensions [44]. The peak resultant is an agreement to the cards (JCPDS card, No. 45-0946) and (JCPDS No. 4-829).

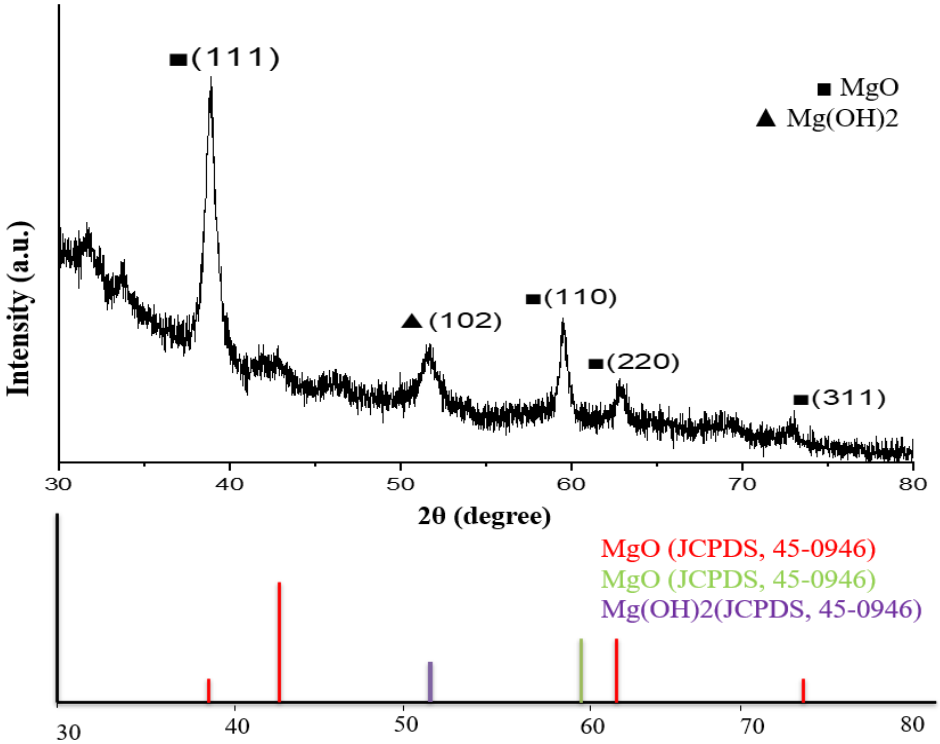

Figure 3: Showing the XRD of MgO NFs deposited on a glass substrate.

Table 1, explains the analyzed sample's orientation, crystalline size, and d-spacing in detail. The peak observed at 2θ° equal to 51.56° is associated with the (102) plane of $Mg(OH)_2$ card no. JCPDS No. 45-0946 [45]. The reason for the presence of magnesium hydroxide related to that $Mg(OH)_2$ is easily formed when MgO is hydrated, covering the MgO surface[46]. The employee determines the average crystalline size of the Scherrer formula [45, 47] as shown in equation (4):

$$D = \frac{0.9\lambda}{\beta Cos\theta} \quad (4)$$

Where D is the average crystalline size, 0.9 is the shape factor constant, λ is the wavelength used as the source (Cu-Kα), β is FWHM, which is the (full width at the half-maximum), θ is the diffraction angle. It can be seen the average size produced for the sample manufactured using the PLA technique was approximately 25 nm.

Table 1: XRD structural parameter of MgO NFs.

POSITION	(HKL)	CRYSTAL. SIZE	D-SPACING	CARD NO.	REF.
38.86	(111)	27.9 nm	2.31536 Å	(JCPDS card, No. 45-0946)	[48]
59.46	(110)	41.0 nm	1.5531 Å	(JCPDS No. 4-829)	[49]
62.83	(220)	17.4 nm	1.47775 Å	(JCPDS card, No. 45-0946)	[50]
73.87	(311)	16.1 nm	1.29698 Å	(JCPDS card, No. 45-0946)	[51]

Using FTIR spectroscopy, Balamurugan et al. [52] studied the MgO NFs and showed the vibrational mode of Mg–O–Mg located between (487–677) cm^{-1} wavenumber region. On the other hand, the previous studies show the MgO stretching vibration mode ~600-850 cm^{-1} [45, 53]. In this study, the peak between 640 cm^{-1} and 715 cm^{-1} is correlated to Mg–O–Mg bonds that confirm the creation of MgO NFs and are indicated with the mentioned references. Water molecules' O-H stretching vibrations are related to the wide vibration band at 3440-3450 cm^{-1}, whereas those at 1630-1640 cm^{-1} are connected with their bending mode [42]. Furthermore, a faint band related to gas-phase CO_2 adsorption is evident at roughly 2375-2385 cm^{-1} due to carbon dioxide from ambient or lab settings. FTIR spectrum of MgO NFs prepared using laser ablation method displayed in Fig. 4.

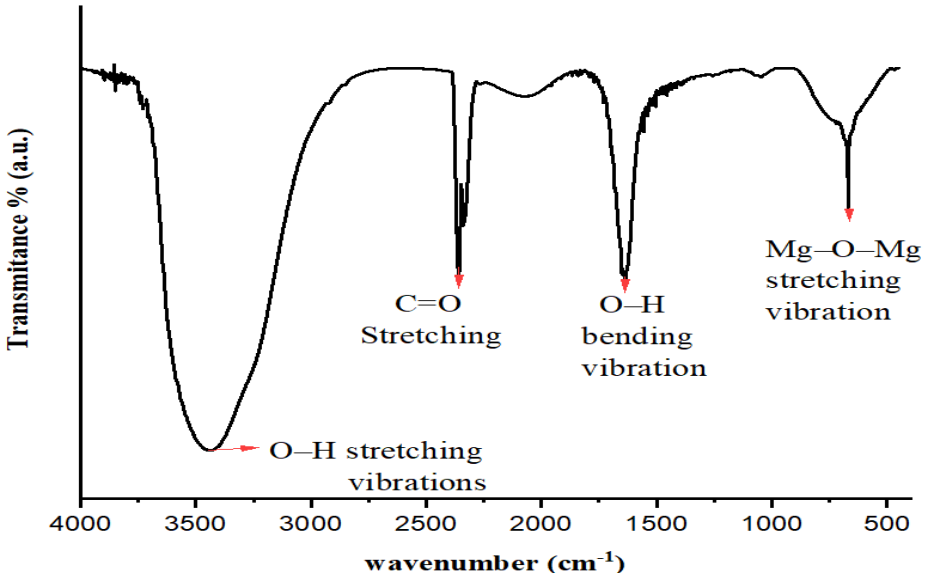

Figure 4: FTIR spectra of MgO NFs suspension prepared using laser ablation in liquid method.

A visible UV spectrophotometer was used to record UV VIS spectra of the synthesized MgO NFs suspension in the absorbance mode represented in Fig 5a. The wavelength ranges between 200–800 nm to determine the absorbance of MgO NFs. MgO NFs absorption region has a wide range beginning from 250 nm to 800 nm. The reality that the peak doesn't appear sharp suggests that this approach produces varying-sized nanoparticles [54]. Tauc's relation [55] can be used to specify the relationship between the photon energy (hυ) and the coefficient (α), which was:

$$(\boldsymbol{\alpha h\upsilon}) = \boldsymbol{A}\,(\boldsymbol{h\upsilon - Eg})^{\boldsymbol{n}} \qquad (5)$$

Where A is a constant relay to the type of the material, Eg is band gap energy, and 'n' is a constant, which is an exponent whose values depend on the electronic transition and range from 1/2 to 3/2, 2 to 3. For the current investigation, the optical band gap was obtained using n = 2 (for the permitted direct transition band gap) where n = 1/m [56]. The absorption coefficient (α) of the magnesium oxide is valued using the mathematical formula [57]:

$$\alpha = 2.303 \frac{A}{d} \quad (6)$$

Where: d is the path length and A absorbance related to the suspended MgO NFs. The band gap of MgO NFs was calculated by plotting the $(\alpha h\upsilon)^2$ versus hυ (eV) as revealed in Fig. 5b. For MgO NFs, a plot between $(\alpha h\upsilon)^2$ and photon energy (hυ) is drawn, considering the direct band transition in MgO NFs. The tangent's intercept shows the direct band gap of MgO NFs to the plot on the X-axis. The optical energy band gap value for the MgO NFs samples (5.8 eV), according to Fig. 5b matched with the previous reference [58]. In the current work, MgO has an optical band gap greater than the bulk value attributed to the quantum confinement effect. The intergranular areas' chemical vacancies or flaws, which create new energy levels to raise the band gap energy, are responsible for this impact [59, 60].

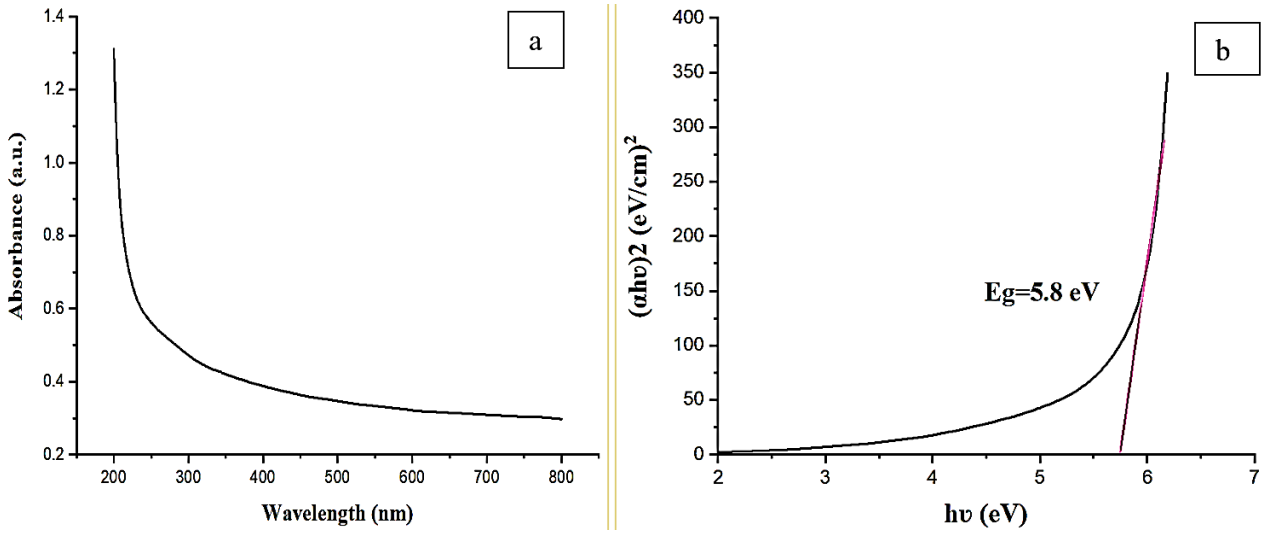

Figure 5: Illustrate (a) UV visible spectra of MgO NFs, (b) estimated band gap.

FESEM images of the MgO NFs suspension deposited on the glass slab are shown in Fig. 6 a. Morphological analysis shows irregular distribution clusters of flake-like nanostructures. These structures sometimes appear branched in nature. These nano flake structures have a typical diameter of 100-400 nm and a very small thickness of the walls around 24 nm. It demonstrates clearly that the vertically aligned MgO NFs grow uniformly on a glass substrate. Most NFs intersect to form a network structure providing a large surface area. It is well documented in the literature that laser ablation in liquid normally produces nanoparticles, with most having sphere-like structures. In the present work the production obtained was nano flakes. Laser ablation method with very high laser energy may exfoliate the surface of magnesium target. This is mostly because the target has a low melting point (650 °C), boiling point (1107 °C), and hardness point [61] hence low ablation threshold. Another proposed reason related to the aging time may reconstructed the structure from spherical to nanorod or nanocubes or nano flakes. The disappearance of the surface plasmon resonance peak support the last reason [62].

The EDX analysis shown in Fig. 6b indicated the existence of Magnesium (Mg), and Oxygen (O) elements in the sample at bending energy 0.5–1.5 keV without any other impurities. This proves the high purity of the manufactured MgO NFs using the laser ablation technique. In the MgO NFs sample, the elemental compositions of O, and Mg were 59.6 %, and 40.4%, respectively.

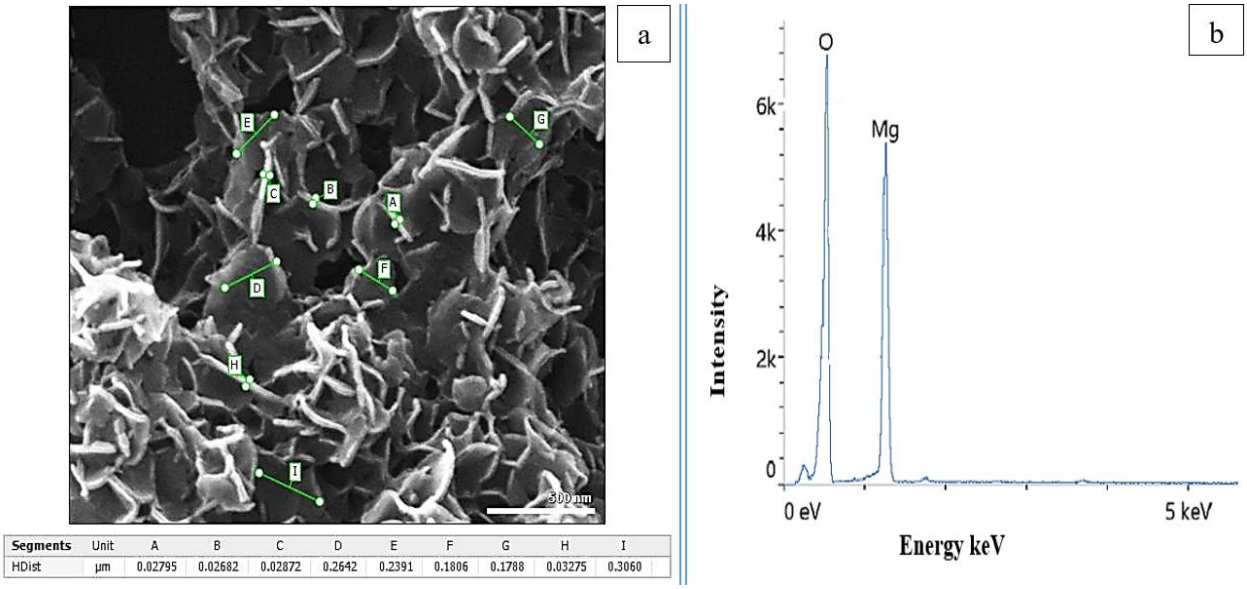

Figure 6: (a) shows the FESEM image of MgO NFs, (b) EDX analysis of composition MgO NFs.

Diffraction light scattering (DLS) was used to identify the hydrodynamic residue and distribution of sizes of MgO NFs in colloidal dispersion illustrated in Fig. 7a. According to the size distribution graph, the average size of the MgO NFs in the dispersion of colloids was 30.59 nm. As demonstrated, the average size of MgO NFs changed depending on the analysis. The particle size determined by DLS was greater than that determined by FESEM and XRD. The observed result may be explained by the variations in the FESEM and DLS analysis circumstances. DLS measurements are carried out in an aqueous environment to account for the difference in particle diameter determination, and FESEM analysis is carried out on dry particles. The hydrodynamic diameter, which represents the size of the particles when they are hydrated, is provided by DLS. The poly-dispersity index of the NFs is provided by the DLS analysis. The DLS analysis provides the poly-dispersity index of the NFs. The range of the PDI scale is 0 to 1 [27]. The suspension homogeneity is indicated by a PDI score of less than (0.4). However, a PDI value of more than one means the suspension is extremely diverse [63]. In this study, the PDI provided was 0.07. This suggests the synthesized NFs' particle size distribution was more homogeneous and narrower. This implies that a sizable fraction of the MgO NFs had comparable sizes, which helped to create a well-defined size distribution. Improved control over the synthesis process, which produces NFs with uniform sizes, is frequently implied by a lower PDI value. The present PDI value is encouraging in general as it suggests that the synthesis procedure produced MgO NFs with comparatively consistent particle sizes. This could be useful for integrating the particles into different applications where a uniform particle size is required. The zeta potential represents the movement of MgO NFs in a dispersion of colloidal particles under the effect of an electric field. In the present investigation, Fig. 7b shows the zeta value (- 36.1 mV) for PLAL MgO NFs, suggesting good stability. The highly stable dispersions present Zeta values of more than ±30 mV. This evidence suggests increased electrostatic repulsion between NFs, assisting in stabilizing and preventing their aggregation. Because of the significant negative charge, there is more electrostatic repulsion between the particles, which lessens the potential for the particles to aggregate and ensures their stability.

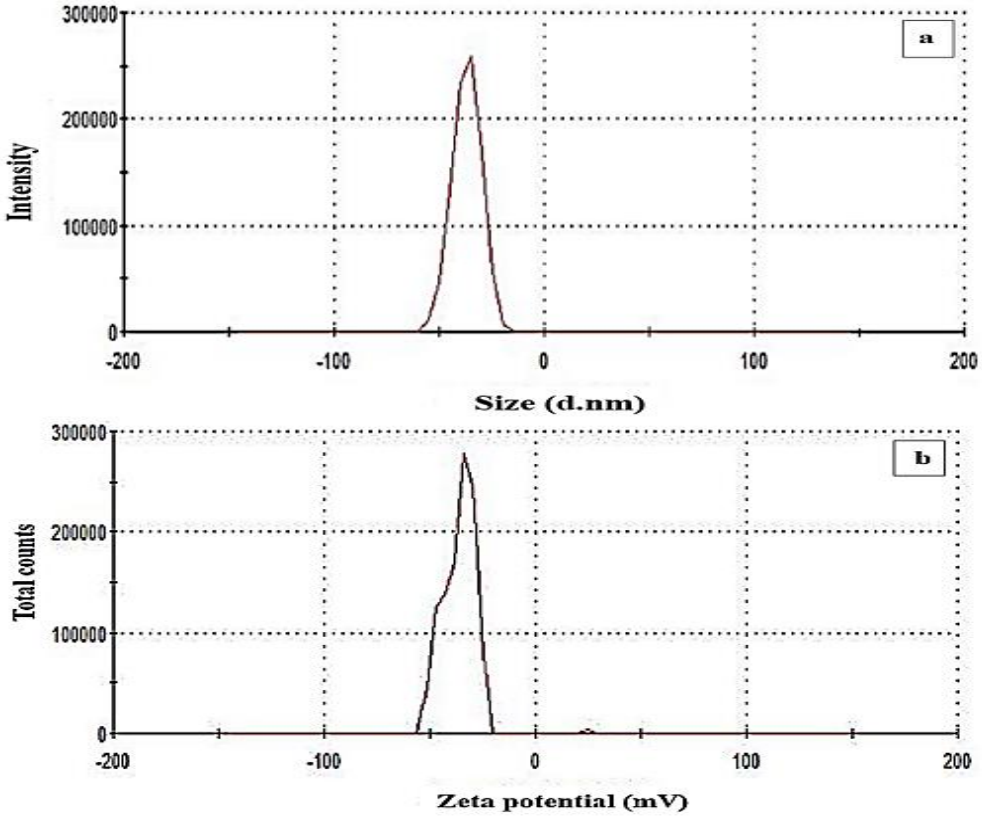

Figure 7: DLS analysis of MgO NFs (a) particle size, (b) zeta potential.

4. Antibacterial Test

Multi-drug resistant microorganisms (MRM) are a significant concern in both agriculture and healthcare. These MRM strains have sophisticated mechanisms that allow them to withstand the effects of antibiotics, making it more difficult to treat and manage their infections. To improve their antimicrobial action, scientists are actively researching new active chemicals like nanoparticles, which have distinct qualities such as their vast surface area, compact size, and capacity to penetrate microbial cells [27, 64]. Magnesium oxide nanoparticles in this work show impressive antibacterial efficacy against Gram-positive and Gram-negative bacteria. It was discovered that the degree of bacterial growth inhibition seen in this investigation varied and depended on concentration. This phenomenon was consistent with several previously published investigations [26, 65]. Fig. 8 shows the antibacterial activity of MgO NFs against *E. coli* and *S. aureus* isolates in different concentration. Different concentrations of MgO NFs (25, 50, 100, 150, and 200) µg/mL were applied to verify the antibacterial activity. The first column represents pure distilled water, and the final one refers to silver nitride ($AgNO_3$) as a control agent. This step was done to compare with the antibacterial activity of MgO NFs. Using the concentrations (150 and 200) µg/mL exceeded the effect of $AgNO_3$. As shown, the highest antibacterial activity was observed at a high MgO NFs concentration (200 µg/mL) with inhibition zones 15 mm ±0.5mm for *E. coli* and 16 mm ±0.5 mm for *S.aureus.* The inhibition zone decreased remarkably to 5 mm±0.5 mm, and 4 mm ±0.5 mm at a concentration (25 µg/mL) for *E. coli* and *S.aureus*, respectively. The minimum inhibitory concentration (MIC) value denotes the smallest amount of the active ingredient required to slow or prevent microbial growth. Determination of (MIC) is a crucial step in investigating the efficacy of active substances and comprehending their ability to combat various pathogenic microorganisms. The choice of antibiotics, concentration optimization, reducing the emergence of antibiotic-resistant microbes, contrasting the antibacterial activities of different compounds, identifying new tactics for battling infectious diseases, aiding in drug formulation and clinical choice, and helping to develop efficient treatment protocols all rely heavily on MIC data [27, 66]. In this study, the MIC for MgO NFs prepared using laser ablation in liquid technique was 25 µg/mL for both pathogens studied. The minimum inhibitory concentration was 25 µg/mL for both pathogens studied. The structure of microbial cell walls is a major factor in explaining MgO NFs' antibacterial action. Compared to Gram-negative bacteria, gram-positive bacteria have a thicker peptidoglycan layer that serves as a barrier preventing MgO NFs

from penetrating [67, 68]. This explains why MgO NFs have greater antibacterial action against gram-negative bacteria than they do against gram-positive bacteria.

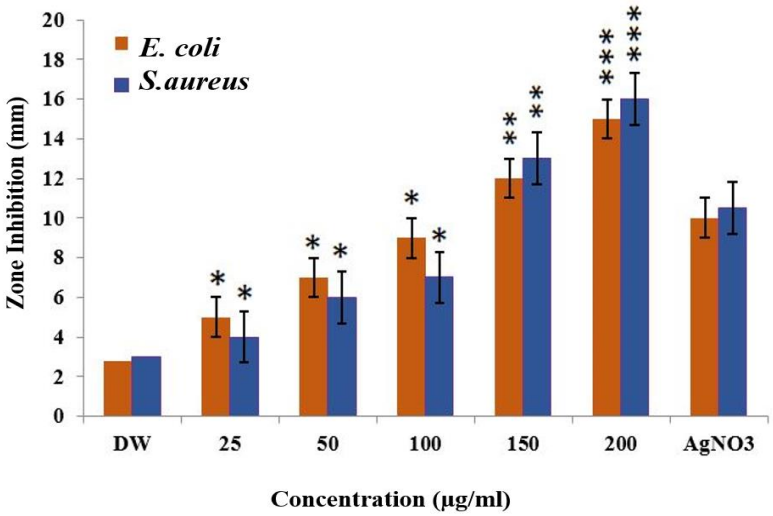

Figure 8: Antibacterial activity of MgO NFs against *E. coli* and *S. aureus*. (DW: distilled water, $AgNO_3$: control agent). Data are presented as (mean ± SD (*p < 0.05; **p < 0.01; ***p < 0.001); n = 3).

5. Conclusion

Pulse laser ablation in liquid could be considered the best and easiest way to create MgO NFs. The results of the characterization technique (XRD, UV visible, FESEM, EDX, DLS, and FTIR) confirm the creation of MgO NFs. These nanostructures were poly crystalline, flake-like in shape, had different diameters reaching 400 nm with an average thickness of approximately 24 nm, and the band gap obtained was wide reach to 5.8 eV. MgO NFs have significant negative charge and high stability. MgO NFs showed remarked antibacterial action versus the two bacterial strains (*S. aureus and E. coli*) with low MIC values (25 µg/mL).

Conflict of Interest

The authors declare that they have no conflict of interest.

References

[1] S. N. Rashid, K. A. Aadim, A. S. Jasim, and A. M. J. M. S. Hamad, "Synthesized zinc nanoparticles via pulsed laser ablation: characterization and antibacterial activity," *Modern Science*, vol. 8, p. 17, 2022.

[2] S. J. Salih and A. K. Smail, "Synthesis, characterization and evaluation of antibacterial efficacy of zinc oxide nanoparticles," *Pharmaceutical*, vol. 3, p. 327-333, 2016.

[3] A. K. Potbhare, R. G. Chaudhary, P. B. Chouke, S. Yerpude, A. Mondal, V. N. Sonkusare *et al.*, "Phytosynthesis of nearly monodisperse CuO nanospheres using Phyllanthus reticulatus/Conyza bonariensis and its antioxidant/antibacterial assays," *Materials Science and Engineering: C*, vol. 99, p. 783-793, 2019.

[4] J. T. Seil and T. J. Webster, "Antimicrobial applications of nanotechnology: methods and literature," *International journal of nanomedicine*, p. 2767-2781, 2012.

[5] S. M. Dizaj, F. Lotfipour, M. Barzegar-Jalali, M. H. Zarrintan, K. Adibkia, "Antimicrobial activity of the metals and metal oxide nanoparticles," *Materials Science*, vol. 44, p. 278-284, 2014.

[6] A. M. Mohammed, I. K. Al-Khateeb, A. J. Haider, R. A. Rahim, U. Hashim, "Preparation of DNA biosensor application from fuel oil waste by functionalization and characterization of MWCNT," *Sensing bio-sensing research*, vol. 16, p. 1-5, 2017.

[7] P. R. Jubu, K. M. Chahrour, Y. Yusof, A. Nathan-Abutu, V. Igba, E. Danladi *et al.*, "An Alternative Method for Estimating the Phase Fraction of Multiphase Nanomaterials: Analysis from X-ray Diffraction," *Journal of Applied Sciences Nanotechnology*, vol. 3, 2023.

[8] P.P.Fedorov, E.A.Tkachenko, S.V.Kuznetsov, V.V.Voronov, and S. V. Lavrishchev, "Preparation of MgO

nanoparticles," *Inorganic Materials,* vol. 43, p. 502-504, 2007.
[9] S. Makhluf, R. Dror, Y. Nitzan, Y. Abramovich, R. Jelinek, and A. Gedanken, "Microwave-assisted synthesis of nanocrystalline MgO and its use as a bacteriocide," *Advanced Functional Materials,* vol. 15, p. 1708-1715, 2005.
[10] A. J. Haider, F. I. Sultan, M. J. Haider, and N. M. Hadi, "Spectroscopic and structural properties of zinc oxide nanosphere as random laser medium," *Applied Physics A,* vol. 125, p. 260, 2019.
[11] I. Djerdj, D. Arčon, Z. Jagličić, and M. Niederberger, "Nonaqueous synthesis of metal oxide nanoparticles: short review and doped titanium dioxide as case study for the preparation of transition metal-doped oxide nanoparticles," *Journal of Solid State Chemistry,* vol. 181, p. 1571-1581, 2008.
[12] T. Selvamani, T. Yagyu, S. Kawasaki, and I. Mukhopadhyay, "Easy and effective synthesis of micrometer-sized rectangular MgO sheets with very high catalytic activity," *Catalysis Communications,* vol. 11, p. 537-541, 2010.
[13] S. S. Batros, M. H. Ali, and A. J. Addie, "Microstructure-Modulated Antibacterial Performance of Chemically Precipitated SnO2 Nanoparticles," *Journal of Applied Sciences Nanotechnology*, vol. 3, 2023.
[14] F. Al-Hazmi, F. Alnowaiser, A. A.Al-Ghamdi, A. A. Al-Ghamdi, M. M.Aly, R. M. Al-Tuwirqi *et al.*, "A new large–scale synthesis of magnesium oxide nanowires: structural and antibacterial properties," *Superlattices Microstructures,* vol. 52, p. 200-209, 2012.
[15] M. Nabiyouni, T. Brückner, H. Zhou, U. Gbureck, and S. B. Bhaduri, "Magnesium-based bioceramics in orthopedic applications," *Acta biomaterialia,* vol. 66, p. 23-43, 2018.
[16] G. Spoto, E. Gribov, G. Ricchiardi, A. Damin, D. Scarano, S. Bordiga *et al.*, "Carbon monoxide MgO from dispersed solids to single crystals: a review and new advances," *Progress in surface science,* vol. 76, p. 71-146, 2004.
[17] D. Varshney, S. Dwivedi, "On the synthesis, structural, optical and magnetic properties of nano-size Zn–MgO," *Superlattices Microstructures,* vol. 85, p. 886-893, 2015.
[18] K. Krishnamoorthy, J. Y. Moon, H. B. Hyun, S. K. Cho, and S.-J. Kim, "Mechanistic investigation on the toxicity of MgO nanoparticles toward cancer cells," *Journal of materials chemistry,* vol. 22, p. 24610-24617, 2012.
[19] J. Sawai, H. Kojima, H. Igarashi, A. Hashimoto, S. Shoji, T. Sawaki *et al.*, "Antibacterial characteristics of magnesium oxide powder," *World Journal of Microbiology* vol. 16, p. 187-194, 2000.
[20] A. Al-Sharabi, K. S. Sada'a, A. Al-Osta, and R. Abd-Shukor, "Structure, optical properties and antimicrobial activities of MgO–Bi2− x Cr x O3 nanocomposites prepared via solvent-deficient method," *Scientific Reports,* vol. 12, p. 10647, 2022.
[21] Y. N. Slavin, J. Asnis, U. O. Hńfeli, and H. Bach, "Metal nanoparticles: understanding the mechanisms behind antibacterial activity," *Journal of nanobiotechnology,* vol. 15, p. 1-20, 2017.
[22] A. Fouda, S. E.-D. Hassan, A. M. Eid, M. A. Abdel-Rahman, and M. F. Hamza, "Light enhanced the antimicrobial, anticancer, and catalytic activities of selenium nanoparticles fabricated by endophytic fungal strain, Penicillium crustosum EP-1," *Scientific Reports,* vol. 12, p. 11834, 2022.
[23] N. B. Basosila, C. L. Inkoto, O. M. Maganga, B. Mbembo, G. N. Kasiama, C. Kabengele *et al.*, "Biogenic Synthesis, Spectroscopic Characterization and Bioactivity of Cymbopogon citratus Derived Silver Nanoparticles," *Journal of Applied Sciences Nanotechnology,* p. 33-41, 2023.
[24] A. J. Haider, F. I. Sultan, and A. Al-Nafiey, "Controlled growth of different shapes for ZnO by hydrothermal technique, " AIP:Conference Series, vol. 1968, 2018.
[25] P. Bhattacharya, A. Dey, and S. Neogi, "An insight into the mechanism of antibacterial activity by magnesium oxide nanoparticles," *Journal of Materials Chemistry B,* vol. 9, p. 5329-5339, 2021.
[26] A. Pugazhendhi, R. Prabhu, K. Muruganantham, R. Shanmuganathan, S. Natarajan, "Anticancer, antimicrobial and photocatalytic activities of green synthesized magnesium oxide nanoparticles (MgONPs) using aqueous extract of Sargassum wightii," *Journal of Photochemistry,* vol. 190, p. 86-97, 2019.
[27] A. Fouda, K. S. Alshallash, M. I. Alghonaim, A. M. Eid, A. M. Alemam, M. A. Awad, *et al.*,"The Antimicrobial and Mosquitocidal Activity of Green Magnesium Oxide Nanoparticles Synthesized by an Aqueous Peel Extract of Punica granatum," *Chemistry,* vol. 5, p. 2009-2024, 2023.
[28] V. Stanić and S. B. Tanasković, "Antibacterial activity of metal oxide nanoparticles," *Nanotoxicity,* , p. 241-274, 2020.
[29] M. A. Al-Kinani, A. J. Haider, and S. Al-Musawi, "High uniformity distribution of Fe@ Au preparation by

a micro-emulsion method," IOP:Conference Series, vol. 987, p. 012013, 2020.
[30] A. J. Haider, M. A. Al-Kinani, and S. Al-Musawi, "Preparation and characterization of gold coated super paramagnetic iron nanoparticle using pulsed laser ablation in liquid method," *Key Engineering Materials*, vol. 886, p. 77-85, 2021.
[31] M. Ramani, S. Ponnusamy, C. Muthamizhchelvan, J. Cullen, S. Krishnamurthy, E. J. C. Marsili, "Morphology-directed synthesis of ZnO nanostructures and their antibacterial activity," *Colloids Surfaces B: Biointerfaces*, vol. 105, p. 24-30, 2013.
[32] A. J. Haider, R. Al-Anbari, G. Kadhim, and Z. Jameel, "Synthesis and photocatalytic activity for TiO2 nanoparticles as air purification," in MATEC : Conference Series, vol. 162, p. 05006, 2018.
[33] A. A. Salih, A. Nazar, and A. J. Haider, "Antibacterial activity of zno nanoparticle prepared by pulsed laser ablation in liquid for biological sensor," IEEE :Conference Series, p. 726-729, 2019.
[34] X. Hong, J. Wen, X. Xiong, and Y. Hu, "Shape effect on the antibacterial activity of silver nanoparticles synthesized via a microwave-assisted method," *Environmental science pollution research*, vol. 23, p. 4489-4497, 2016.
[35] L. Wang, H. He, Y. Yu, L. Sun, S. Liu, C. Zhang, and L. He, "Morphology-dependent bactericidal activities of Ag/CeO2 catalysts against Escherichia coli," *Journal of inorganic biochemistry*, vol. 135, p. 45-53, 2014.
[36] K. D. Salman, H. H. Abbas, and H. A. Aljawad, "Synthesis and characterization of MgO nanoparticle via microwave and sol-gel methods," Journal of Physics:Conference Series, vol. 1973, p. 012104, 2021.
[37] K. Gopalakrishnan, H. M. Joshi, P. Kumar, L. Panchakarla, and C.N.R. Rao, "Selectivity in the photocatalytic properties of the composites of TiO2 nanoparticles with B-and N-doped graphenes," *Chemical Physics Letters*, vol. 511, p. 304-308, 2011.
[38] Y. Chen, X. Tian, W. Zeng, X. Zhu, H. Hu, and H. Duan, "Vapor-phase preparation of gold nanocrystals by chloroauric acid pyrolysis," *Journal of colloid*, vol. 439, p. 21-27, 2015.
[39] X. Wu, L. Zheng, and D.Wu, "Fabrication of superhydrophobic surfaces from microstructured ZnO-based surfaces via a wet-chemical route," *Langmuir*, vol. 21, p. 2665-2667, 2005.
[40] M. Rezaei, M. Khajenoori, and B. Nematollahi, "Synthesis of high surface area nanocrystalline MgO by pluronic P123 triblock copolymer surfactant," *Powder technology*, vol. 205, p. 112-116, 2011.
[41] E. A. Mwafy and A. M. Mostafa, "Efficient removal of Cu (II) by SnO2/MWCNTs nanocomposite by pulsed laser ablation method," *Nano-Structures*, vol. 24, p. 100591, 2020.
[42] A. J. Haider, T. Alawsi, M. J. Haider, B. A. Taha, and H. A. Marhoon, "A comprehensive review on pulsed laser deposition technique to effective nanostructure production: Trends and challenges," *Optical Quantum Electronics*, vol. 54, p. 488, 2022.
[43] E. A. Mwafy and A. M. Mostafa, "Multi walled carbon nanotube decorated cadmium oxide nanoparticles via pulsed laser ablation in liquid media," *Optics*, vol. 111, p. 249-254, 2019.
[44] C. F. Holder and R. E. Schaak, "Tutorial on powder X-ray diffraction for characterizing nanoscale materials," *Acs Nano*, vol. 13, p. 7359-7365, 2019.
[45] N. C. S. Selvam, R. T. Kumar, L. J. Kennedy, and J. J. Vijaya, "Comparative study of microwave and conventional methods for the preparation and optical properties of novel MgO-micro and nano-structures," *Journal of Alloys*, vol. 509, p. 9809-9815, 2011.
[46] L. Huang, D. Li, Y. Lin, D. G. Evans, and X. Duan, "Influence of nano-MgO particle size on bactericidal action against Bacillus subtilis var. niger," *Chinese science bulletin*, vol. 50, p. 514-519, 2005.
[47] A. A. Yousif, N. F. Habubi, and A.J. Haidar, "Nanostructure zinc oxide with cobalt dopant by PLD for gas sensor applications," *Journal of Nano- and Electronic Physics*,vol. 4, p. 02007, 2012.
[48] S. Yousefi and B. Ghasemi, "Precipitator concentration-dependent opto-structural properties of MgO nanoparticles fabricated using natural brine," *J SN Applied Sciences*, vol. 2, p. 1-10, 2020.
[49] N. K. Nga, N. T. T. Chau, and P. H. Viet, "Preparation and characterization of a chitosan/MgO composite for the effective removal of reactive blue 19 dye from aqueous solution," *Advanced Materials Devices*, vol. 5, p. 65-72, 2020.
[50] F. A. Fadhil, J. M. Taha, K. S. Khashan, and F. Mahdi, "Optical properties of MgO NPs produced by laser ablation in liquid," AIP: Conference Series, vol. 2372, 2021.
[51] M. M. Obeid, S. J. Edrees, and M. M. Shukur, "Synthesis and characterization of pure and cobalt doped magnesium oxide nanoparticles: insight from experimental and theoretical investigation," *Superlattices*

Microstructures, vol. 122, p. 124-139, 2018.
[52] S. Balamurugan, L. Ashna, and P. Parthiban, "Synthesis of nanocrystalline MgO particles by combustion followed by annealing method using hexamine as a fuel," *Journal of nanotechnology,* vol. 2014, 2014.
[53] G. Balakrishnan, R. Velavan, K. M. Batoo, and E. H. Raslan, "Microstructure, optical and photocatalytic properties of MgO nanoparticles," *Results in Physics,* vol. 16, p. 103013, 2020.
[54] L. Aghebati-maleki, B. Salehi, R. Behfar, H. Saeidmanesh, F. Ahmadian, M. Sarebanhassanabadi, et al., "Designing a hydrogen peroxide biosensor using catalase and modified electrode with magnesium oxide nanoparticles," *Int. J. Electrochem. Sci,* vol. 9, p. 257-271, 2014.
[55] A. J. Haider, A. A. Jabbar, and G. A. Ali, "A review of pure and doped ZnO nanostructure production and its optical properties using pulsed laser deposition technique," Journal of Physics: Conference Series, vol. 1795, p. 012015, 2021.
[56] Atul, M. Kumar, A. Sharma, I. K. Maurya, A. Thakur, and S. Kumar, "Synthesis of ultra small iron oxide and doped iron oxide nanostructures and their antimicrobial activities," *Journal of Taibah University for Science,* vol. 13, p. 280-285, 2019.
[57] M. Dar and D. Varshney, "Structures and properties of Mg 0.95 Mn 0.01 TM 0.04 O (TM= Co, Ni, and Cu) nanoparticles synthesized by sol–gel auto combustion technique," *The Royal Society of Chemistry,* vol. 8, p. 14120-14128, 2018.
[58] R. Sreekanth, J. Pattar, A. V. Anupama, and A. M. M. Mallikarjunaswamy, "Synthesis of high surface area and plate-like Magnesium Oxide nanoparticles by pH-controlled precipitation method," *Applied Physics A,* vol. 127, p. 797, 2021.
[59] H. Yamamoto, S. Tanaka, and K. Hirao, "Effects of substrate temperature on nanostructure and band structure of sputtered Co 3 O 4 thin films," *Journal of applied physics,* vol. 93, p. 4158-4162, 2003.
[60] L. Soriano, M. Abbate, J. Vogel, J. Fuggle, A. Fernández, A. González-Elipe *et al.,* "The electronic structure of mesoscopic NiO particles," *Chemical physics letters,* vol. 208, p. 460-464, 1993.
[61] J. Chen, L. Tan, X. Yu, I. P. Etim, M. Ibrahim, and K. Yang, "Mechanical properties of magnesium alloys for medical application: A review," *Journal of the Mechanical Behavior of Biomedical Materials,* vol. 87, p. 68-79, 2018.
[62] K. Zhang, R. A. Ganeev, G. S. Boltaev, P. V. Redkin, and C. Guo, "Effect of different hardness and melting point of the metallic surfaces on structural and optical properties of synthesized nanoparticles," *Materials Research Express,* vol. 6, p. 045027, 2019.
[63] M. Danaei, M. Dehghankhold, S. Ataei, F. Hasanzadeh Davarani, R. Javanmard, A. Dokhani *et al.,* "Impact of particle size and polydispersity index on the clinical applications of lipidic nanocarrier systems," *Pharmaceutics,* vol. 10, p. 57, 2018.
[64] R. Jabbar and N. N. Hussein, "Evaluation the antibacterial activity of biosynthesis silver nanoparticles by lactobacillus gasseri bacteria," *Journal of Applied Sciences Nanotechnology,* vol. 1, p. 86-95, 2021.
[65] M. Vergheese and S. K. Vishal, "Green synthesis of magnesium oxide nanoparticles using Trigonella foenum-graecum leaf extract and its antibacterial activity," *Journal of pharmacognosy,* vol. 7, p. 1193-1200, 2018.
[66] B. Kowalska-Krochmal and R. Dudek-Wicher, "The minimum inhibitory concentration of antibiotics: Methods, interpretation, clinical relevance," *Pathogens,* vol. 10, p. 165, 2021.
[67] S. E.-D. Hassan, A. Fouda, E. Saied, M. M. Farag, A. M. Eid, M. G. Barghoth *et al.,* "Rhizopus Oryzae-mediated green synthesis of magnesium oxide nanoparticles (MgO-NPs): A promising tool for antimicrobial, mosquitocidal action, and tanning effluent treatment," *Journal of Fungi,* vol. 7, p. 372, 2021.
[68] S. F. Abbas, A. J. Haider, and S. Al-Musawi, "Antimicrobial and Wound Healing Effects of Metal Oxide Nanoparticles Enriched Wound Dressing," *Nanomaterials,* 2023.